SOME PRACTICAL ASPECTS OF THE BURST OF LAMINAR SEPARATION BUBBLES

N. Kamiya, S. Suzuki, M. Nakamura and T. Yoshinaga
National Aerospace Laboratory
Tokyo, Japan

Abstract

In this paper results are described of experiments involving the burst of laminar separation bubbles in the flows around an airfoil of a large angle of attack, a circular cylinder and a cone cylinder. Firstly, results of detailed measurements of the change in stalling characteristics of NACA 9324 as they occur with a varying Reynolds number are described, and the aerodynamic mechanism of it is discussed in connection with the occurrence of the burst of bubbles. Secondly, an experiment was conducted on the flow around a circular cylinder involving the burst of bubbles. It was found from the experiment that the drag coefficient decreases discontinuously at the critical values of the Reynolds number, contrary to the description of many textbooks and handbooks where the abrupt change of the drag coefficient at this Reynolds number is continuous. Finally, an experiment was conducted on the force acting on a cone cylinder placed in the flow at an angle of attack of 90°. The side force acting on it is discussed in connection with the existence of laminar separation bubbles.

I. Introduction

The burst of a laminar separation bubble is well-known as a cause of leading edge stall of an airfoil. This phenomenon appears also in the flow around various kinds of cylinders put to practical use, causing a sudden change of forces acting on the cylinders and is thus an important one. In this paper results are described of a line of experiments involving the burst of bubbles in the flows around an airfoil of a large angle of attack, a circular cylinder and a cone cylinder.

The commencement of the works described in this paper was the detailed measurement of the stalling characteristics of an airfoil. The stalling characteristics of airfoil sections are classified into three main types[1] trailing edge stall, leading edge stall and thin airfoil stall. This experiment was planned in order to understand the aerodynamic mechanisms of the change of types from leading edge stall to trailing edge stall. We found that the discontinuous variations of the aerodynamic characteristics of an airfoil and hysteresis are the essential phenomena accompanying the burst of bubbles.

The drag coefficient C_D of a circular cylinder is one of the fundamental subjects of fluid dynamics and has been measured since the 1910's [2]-[6]. But the detailed behavior of a cylinder in the critical range of the Reynolds number has not yet been clarified. Many textbooks and handbooks describe the C_D variation of a circular cylinder with the Reynolds number. In these books C_D decreases gradually as the Reynolds number increases, and decreases abruptly but continuously at a Reynolds number value of about 3×10^5, thereafter increasing gradually.

In 1964, however, Tani[7] pointed out that for a cylinder the transition from subcritical to supercritical range is much more discontinuous than previously reported. In 1969 Bearman[8] measured the base drag coefficient C_{pb} of a cylinder at Reynolds number values ranged from 2×10^5 to 7.5×10^5 and showed that the discontinuity was recorded at $Re \doteqdot 3.4 \times 10^5$.

Based on the results of the experiment on the stalling characteristics mentioned above, we became convinced that the drag also varies discontinuously at the critical Reynolds number. Then we measured in detail the aerodynamic force acting on a circular cylinder at the critical values of the Reynolds number. We found that the drag really varies discontinuously. Further we confirmed that lift force appeared due to the asymmetry of the flow caused by the burst of the bubble on one surface while the bubble on the other surface remained without bursting, which Bearman had mentioned about.

The authors expected that if this lift force acts on a section of a circular cone at a condition where the Reynolds number based on the local diameter of the section is critical, it could be the origin of the flat-spin[9] experienced at tha air drop test of a sounding rocket payload models, which was conducted by the National Space Development Agency of Japan. In order to examin this expectation a measurement has been made on the force acting on a cone-cylinder.

II. Stalling Characteristics of NACA 9324

1. Wind Tunnel and Model

The wind tunnel is the pilot tunnel of the NAL's large low speed wind tunnel[10]. The height and width of the test section are 650 mm and 550 mm respectively.

The two dimensional model was mounted spanning the 550 mm width of the tunnel. The airfoil section decided on was an NACA 9324 according to the following principle;

(1) C_L max has its maximum value in the Reynolds number range of 0.5×10^5 to 4×10^5.

(2) The airfoil must be known widely.

Static pressure orifices are installed at the center line and the slant orifices in Fig. 1 are installed along a line 21.5 mm from the center line; separation points are detected by measuring the pressure difference between the pair of slant orifices. These slant orifices, however, have not been used for most of the experiments due to the time consumed in this measurement.

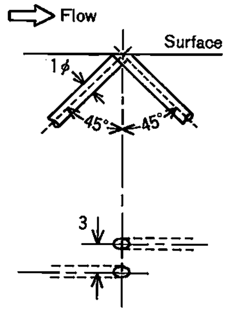

Fig. 1 Slant orifices

2. Test Conditions

Three kinds of experiments have been conducted. Firstly, the Reynolds number was varied from 0.6 x 10^5 to 4 x 10^5 at constant angles of attack of 0°, 5°, 10°, 15° and 20°. Pressure was measured at the static pressure orifices and the slant orifices. After this experiment was finished, it was recognized that more detailed measurement would be necessary in order to understand the whole stalling characteristics of the airfoil, which resulted in the second experiment. The Reynolds number was changed from 0.3 x 10^5 to 4.0 x 10^5 at constant angles of attack ranging from -4° to 36° at every 4 degrees.

In the third experiment the angle of attack was varied ranging from -4° to 40° at constant Reynolds numbers of 0.68, 0.80, 1.05, 1.62, 1.91, 2.23, 2.43, 2.51, 2.56, 2.67, 3.04, 3.42 and 3.82. In the second and third experiments, however, the measurement of pressure at the slant orifices was omitted in order to finish the experiments within the planned period of time.

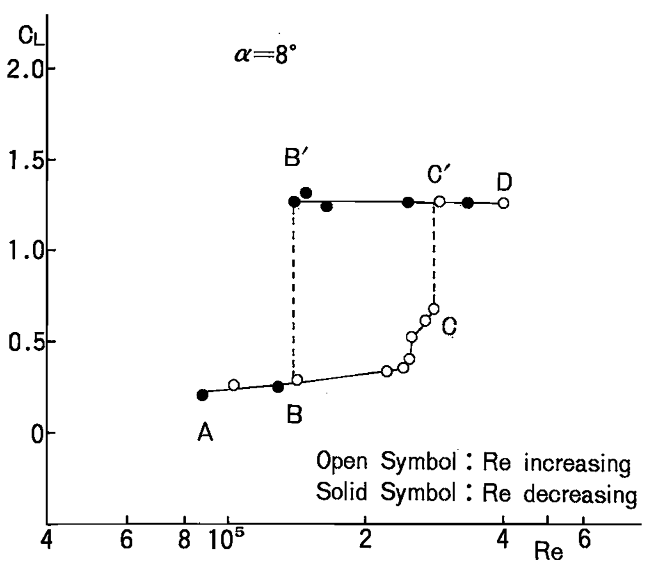

Fig. 2 Variation of C_L with Reynolds number at α = 8°

3. Results and discussions

(1) C_L - R_e Characteristics, hysteresis penomena

Fig. 2 shows a variation of the lift coefficient with a Reynolds number at an angle of attack of 8°. As the Reynolds number increases, C_L varies along the curve A B C C' D, but C_L varies along the curve D C' B' B A as the Reynolds number decreases, so the C_L - R_e curve shows hysteresis loop.

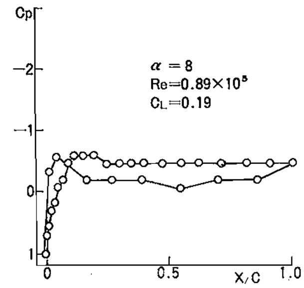

(a) At point A in Fig. 2

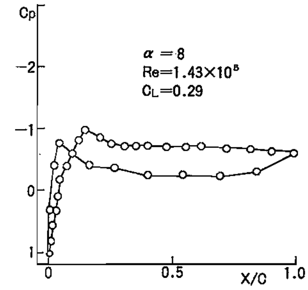

(b) At point B in Fig. 2

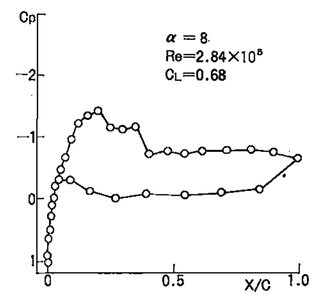

(c) At point C in Fig. 2

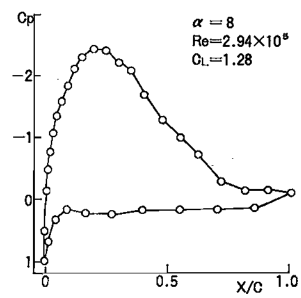

(d) At point C' in Fig. 2

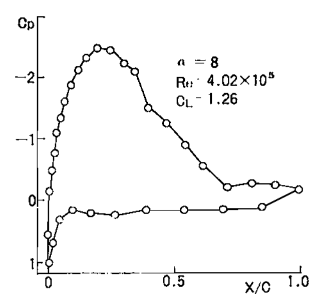

(e) At point D in Fig. 2

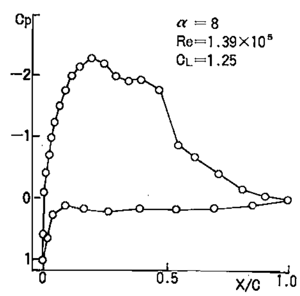

(f) At point B' in Fig. 2

Fig. 3 Pressure distributions of NACA 9324

Fig. 3 shows pressure distributions at Reynolds numbers corresponding to the points A, B, C, C', D and B'. The discussions in Ref. 11 suggest that there is no bubble at the points A, B and C, and bubbles do exist on the upper surface at the points B', C' and D. The jump from B' to B is due to the burst of a bubble and the jump from C to C' is due to the formation of a bubble by reason of the attachment of the separated boundary layer. The results for several attack angles are shown in Fig. 4.

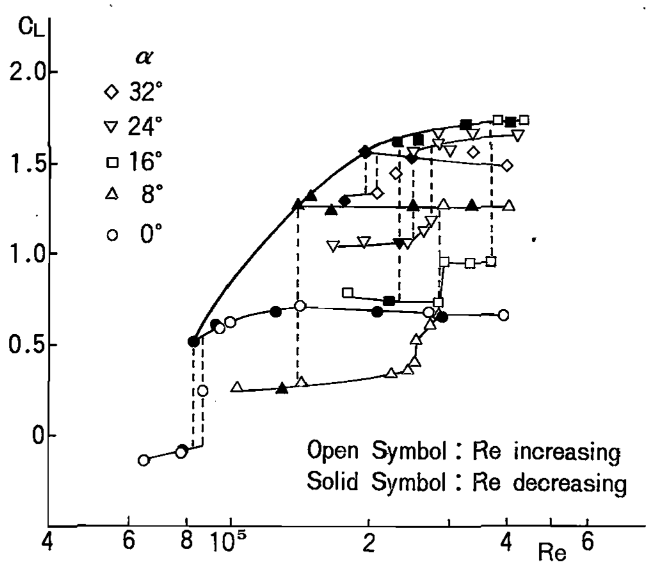

Fig. 4 Variation of C_L with Reynolds number at various angles of attack
Variation of $C_{L\,max}$ with Reynolds number

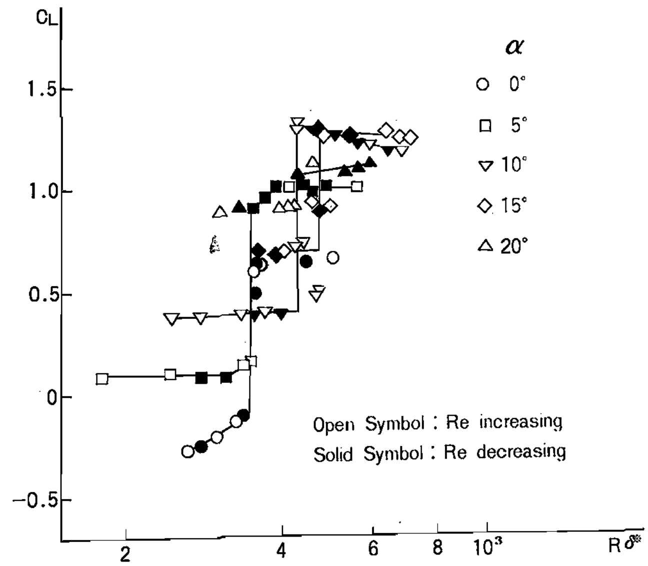

Fig. 5 Variation of C_L with R_{δ^*} at various angles of attack

The C_{lmax} - Re curve is also shown in this figure as the upper limit of all curves except for the portion where the laminar boundary layer separates without reattaching again (line ABC in Fig. 2).

In Fig. 5 C_L is plotted against R_{δ^*}, where R_{δ^*} is a Reynolds number based on the displacement thickness δ^* of the boundary layer at the laminar separation point. δ^* is calculated by use of Thwaite's[12] method using the experimental pressure distribution, where the laminar separation point is determined from the measurement of the difference of the pressure between the pair of slant orifices.

The value of the Reynolds number corresponding to the jump of C_L lies within the range of from 350 to 480, the value of which coincides with the criterion of Tani[13], Owen and Klanfer[14], irrespective of the attack angle and whether the Reynolds number is increasing or decreasing.

Further, the fact that hysteresis phenomena disappear where R_{δ^*} is taken as the abscissa, shows that the formation of a bubble due to the attachment of the separated boundary layer, occurs at the same Reynolds number of about 400 as the bursting of a bubble.

As shown in Fig. 4, the value of the Reynolds number at which a bubble bursts (point B' in Fig. 2) depends on the attack angle. The solid line of Fig. 6 shows the relation between them. In order words this curve shows the locus of the point at which R_{δ^*} = 400 holds. We will hereafter call this curve the stalling curve.

In this figure also shown is the locus of the point where the formation of a bubble occurs (point C in Fig. 2) by a dotted line, which is hereby referred to as the recovery curve. The points A, B, B', C, C' and D in Fig. 2 correspond to A, B, B', C, C' and D in this figure.

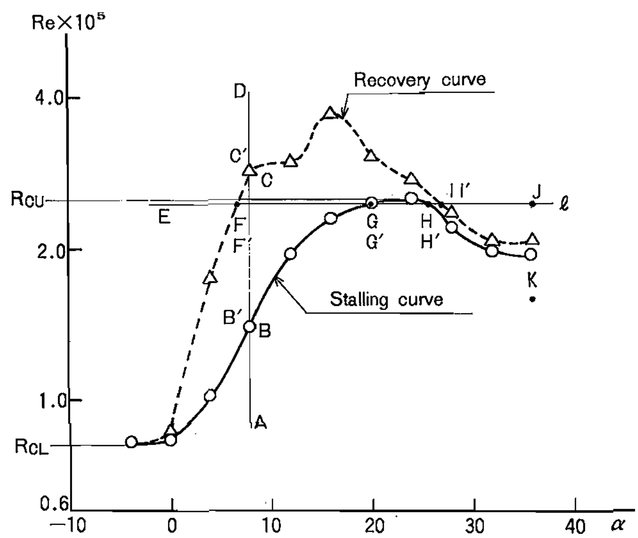

Fig. 6 Stalling curve and recovery curve for constant angle of attack

(2) C_L - α characteristics

The curves in Fig. 6 are the locus of the point where C_L varies discontinuously with the Reynolds number keeping the angle of attack constant. Consider the case where the angle of attack varies keeping the Reynolds number on the horizontal straight line ℓ in this figure. Fig. 7 shows a variation of the lift coefficient with the angle of attack where (c) shows the variation at this Reynolds number. As the angle of attack increases C_L varies along the curve E, G, G', I, I' and J in Fig. 7(c), but varies along the curve J, H', H, F', F and E as the angle of attack decreases. Fig. 8 shows the pressure distributions at the angles of attack corresponding to the points E, G, G', I, I', J, H', H, F' and F. The pressure distributions show that there is no bubble at the points F', G', H and I and bubbles do exist at the points F, G, H', I' and J. The jump of C_L from G to G' is due to the burst of the bubble as shown in (b) and (c) of Fig. 7. This fact is in accordance with the explanation on the stalling curve. If one crosses the stalling curve from left to right at the point G, the bubble on the surface should burst, since a Reynolds number of $R_{\delta *}$ based on the displacement thickness at the laminar separation point is lower than 400 in the region below this curve.

It is remarkable that C_L increases discontinuously at the point I in Fig. 6. The pressure distributions in Fig. 8 (d) and (e) show that this jump is due to the re-formation of a bubble on the upper surface at this value of the attack angle. In Fig. 8 (f) circles show the pressure distribution at point J and x dots show that at point K in Fig. 7 (b), where the angle of attack and the value of C_L for both cases are the same. The fact, that these two distributions are quite different, demonstrate the existence of a bubble at point J. This fact is also in accordance with the explanation on the recovery curve.

If one crosses the recovery curve from left to right at the point I in Fig. 6, the formation of a bubble should occur on the upper surface, since a Reynolds number of $R\delta *$ is higher than

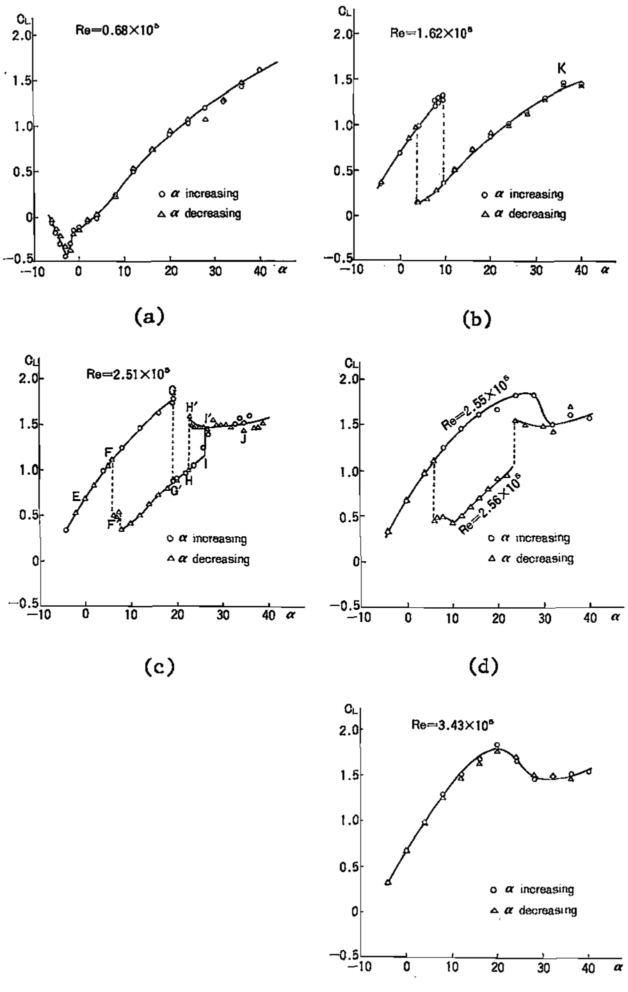

(a) (b) (c) (d) (e)

Fig. 7 Lift characteristics

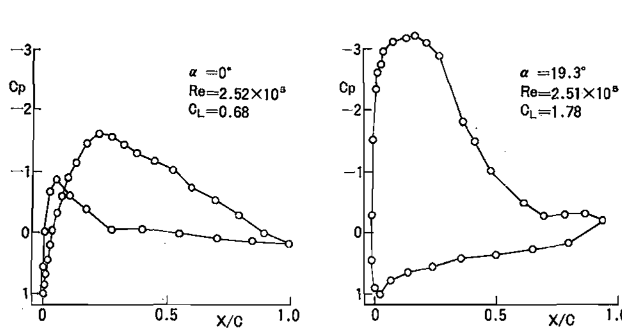

(a) At point E in Fig. 7(c)

(b) At point G in Fig. 7(c)

Fig. 8 Pressure distributions of NACA 9324

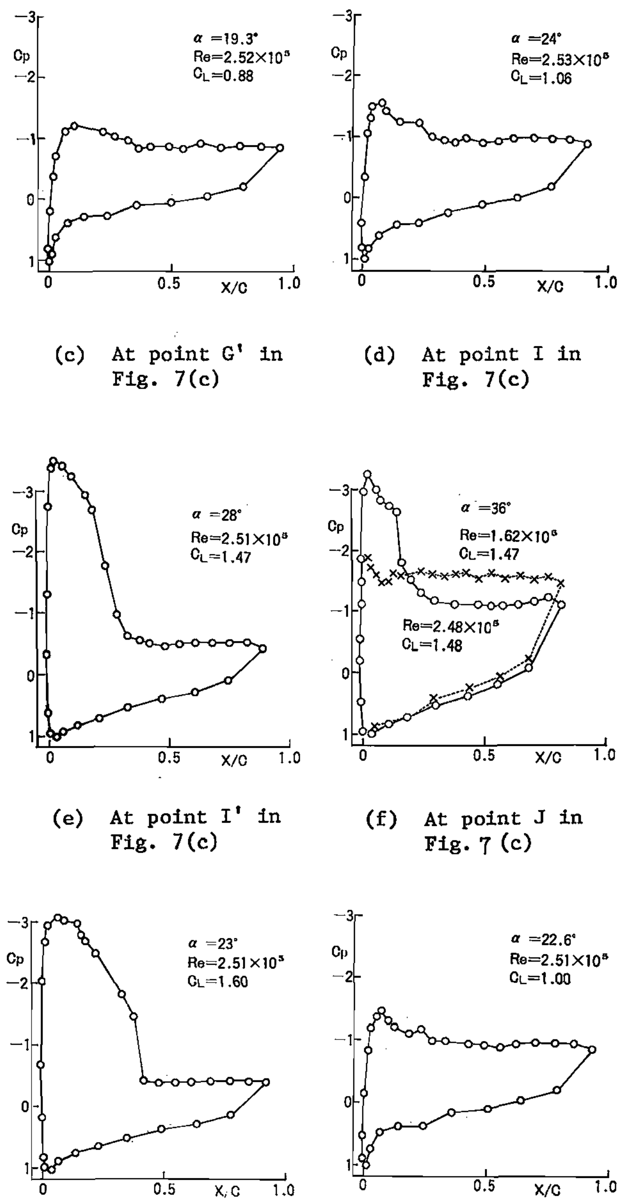

(c) At point G' in Fig. 7(c)

(d) At point I in Fig. 7(c)

(e) At point I' in Fig. 7(c)

(f) At point J in Fig. 7 (c)

(g) At point H' in Fig. 7(c)

(h) At point H in Fig. 7(c)

Fig. 8 (Continued)

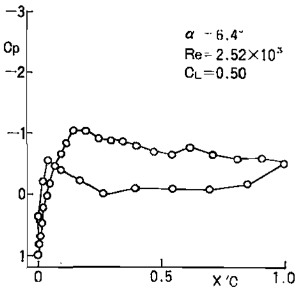

(i) At point F' in Fig. 7(c)

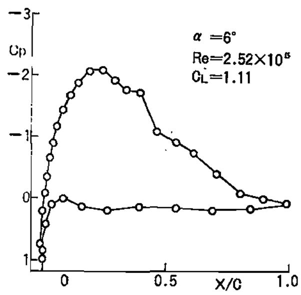

(j) At point F in Fig. 7(c)

Fig. 8 (continued)

400 in the region above this curve. Similarly at the point H in Fig. 6, C_L decreases discontinuously due to the burst of the bubble and at the point F C_L increases discontinuously due to the formation of the bubble, as the angle of attack decreases along the line ℓ.

The values of the Reynolds number corresponding FF', GG', HH' and II' in Fig. 7(c) are slightly different from those corresponding to F, G, H and I in Fig. 6 due to the scatter of measurements. In Fig. 9 stalling and recovery curves are plotted for α variation, keeping the Reynolds number constant. The curves in Figs. 6 and 9 are the same, within the accuracy of the experiment, with the exception that there is no recovery curve above line d in Fig. 9. If the angle of attack increases at a Reynolds number above a critical value, R_{CU} in Fig. 9 the Re - α locus, straight line e for instance, does not intersect with the stalling curve so that the bubble never bursts. The recovery curve, which is the locus of the point where the formation of a bubble occurs, loses its meaning in this case. R_{CU} is hereby referred to as the upper critical Reynolds number, the value of which is 2.56 x 10^5 in this experiment. The C_L - α curve in this case is shown in Fig. 7(e).

When the angle of attack was increased at a Reynolds number of 2.56 x 10^5, the Re - α locus did not intersect with the stalling curve so that the bubble on the surface did not burst. When the angle of attack was decreased on the same run of the experiment, however, the value of the Reynolds number decreased a little to 2.55 x 10^5. The Re - α locus then intersected with the stalling curve resulting in the burst of the bubble so that C_L decreased discontinuously at an angle of attack of 22° as shown in Fig. 7(d).

There is another critical value, R_{CL}. At a Reynolds number below R_{CL}, a bubble does not exist on the upper surface since $R\delta^*$ does not exceed 400 in this case. An example of a C_L - α curve illustrating this case is shown in Fig. 7 (a). R_{CL} is hereby referred to as the lower critical Reynolds number. In this case R_{CL} is about 0.8 x 10^5.

The abrupt decrease of lift coefficient at angle of attack from -6° to -3° is due to the attachment of the boundary layer on the lower surface. The detailed discussion of the boundary layer on the lower surface is not presented in this paper. In the case of Fig. 7(a) the stalling phenomenon did not appear within the range of the experiment, where stalling phenomenon means the loss of lift due to the separation of the boundary layer on the upper surface.

(3) C_L - α - R_e characteristics

Fig. 10 shows the bird's-eye view of the variation of C_L - α characteristics with the Reynolds number. Only the cases, where angle of attack is increasing, are shown here.

According to the above discussions and Fig. 10, C_L - α - R_e characteristics of the NACA 9324 section is summarized as follows: There are two critical Reynolds numbers; the lower critical Reynolds number R_{CL} and the upper critical Reynolds number R_{CU}. At a Reynolds number below R_{CL} a bubble does not exist on the upper surface of the airfoil and the airfoil does not stall within the range of an attack angle below 40°. The difference between the C_L - α characteristics at Reynolds numbers above and below R_{CL} is not

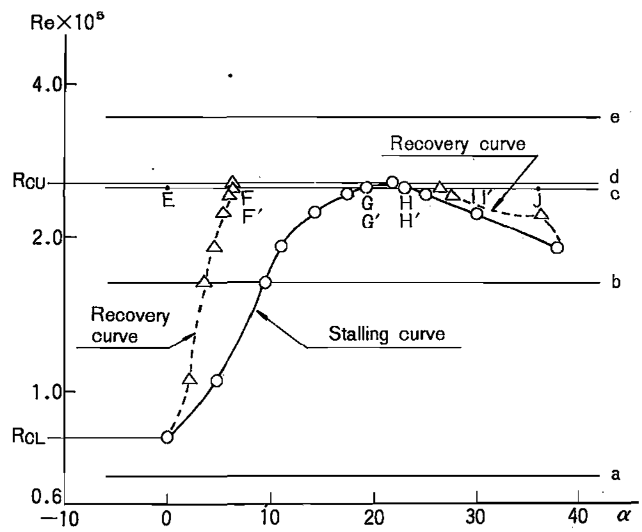

Fig. 9 Stalling curve and recovery curve for constant Reynolds number

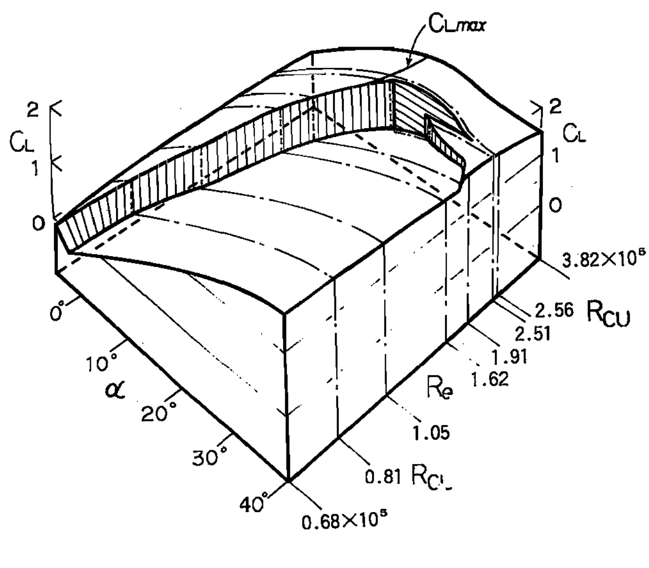

Fig. 10 Bird's-eye view of C_L - α - Re characteristics

clear in this case, where the abrupt decrease of C_L at the Reynolds number below R_{CL} is due to the attachment of the boundary layer on the lower surface, while the discontinuous decrease of C_L at the Reynolds number above R_{CL} is due to the burst of a laminar separation bubble on the upper surface. At a Reynolds number between R_{CL} and R_{CD}, the type of stall is a leading edge stall caused by the burst of a bubble. The remarkable feature in this case is the discontinuous increase of C_L due to the re-formation of a bubble at a high angle of attack ranging from 25° to 40° and a Reynolds number ranging from 1.9 to 2.6 x 10^5. At a Reynolds number above R_{CU} the bubble on the upper surface never burst so that the type of stall is a trailing edge stall caused by the separation of a turbulent boundary layer. The change from a leading edge stall to a trailing edge stall occurs discontinuously as shown in Fig. 10.

III. Aerodynamic Force Acting on a Circular Cylinder

1. Wind tunnel and model

The wind tunnel is the NAL 2m x 2m gust tunnel[15]. The wind velocity ranges from 3 m/s to 60 m/s and the turbulence level is about 0.2 percent.

The model is a circular cylinder whose diameter and span are 0.26m and 2m respectively. It is set up vertically from the floor to the ceiling. The Reynolds number based on the diameter ranges from 1 x 10^5 to 1 x 10^6. Static pressure orifices are installed in the center section at intervals of five degrees. Drag and lift are obtained by integrating the measured pressure on those orifices, and corrections for blockage are made.

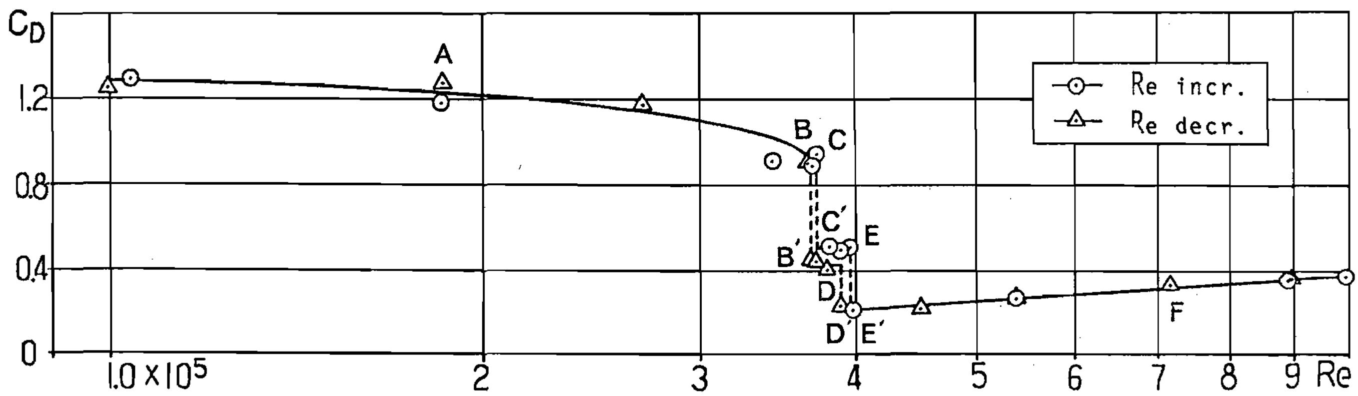

Fig. 11 Variation of drag coefficient of a circular cylinder with the Reynolds number

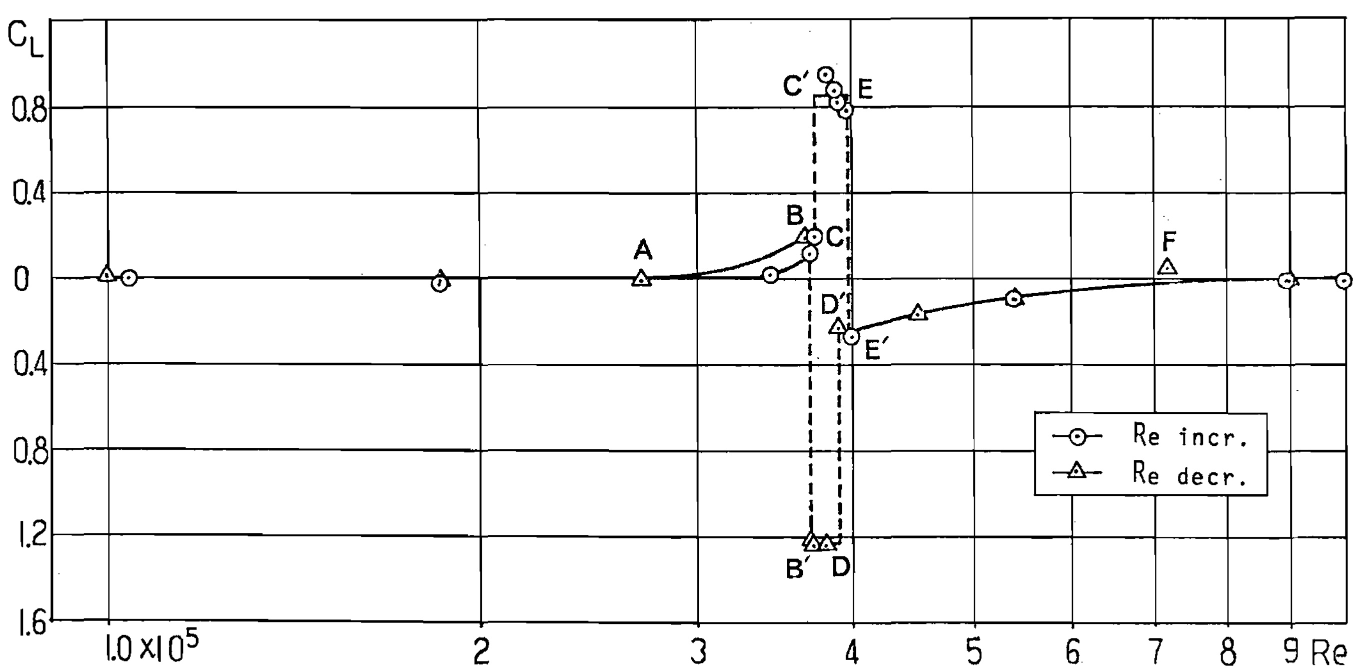

Fig. 12 Variation of lift coefficient of a circular cylinder with the Reynolds number

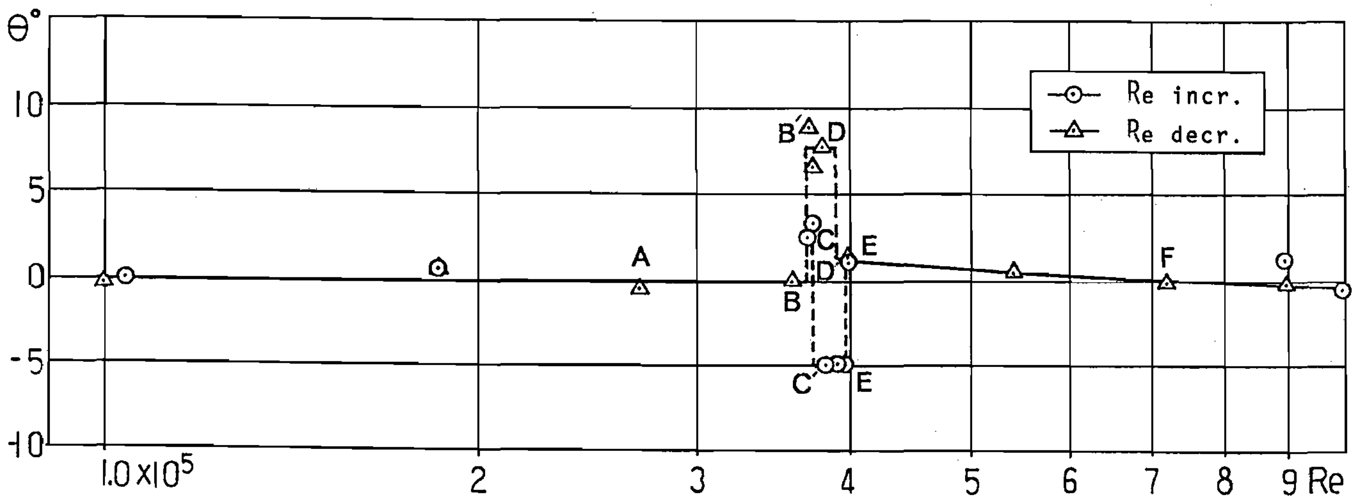

Fig. 13 Variation of the location of stagnation point of a circular cylinder with the Reynolds number

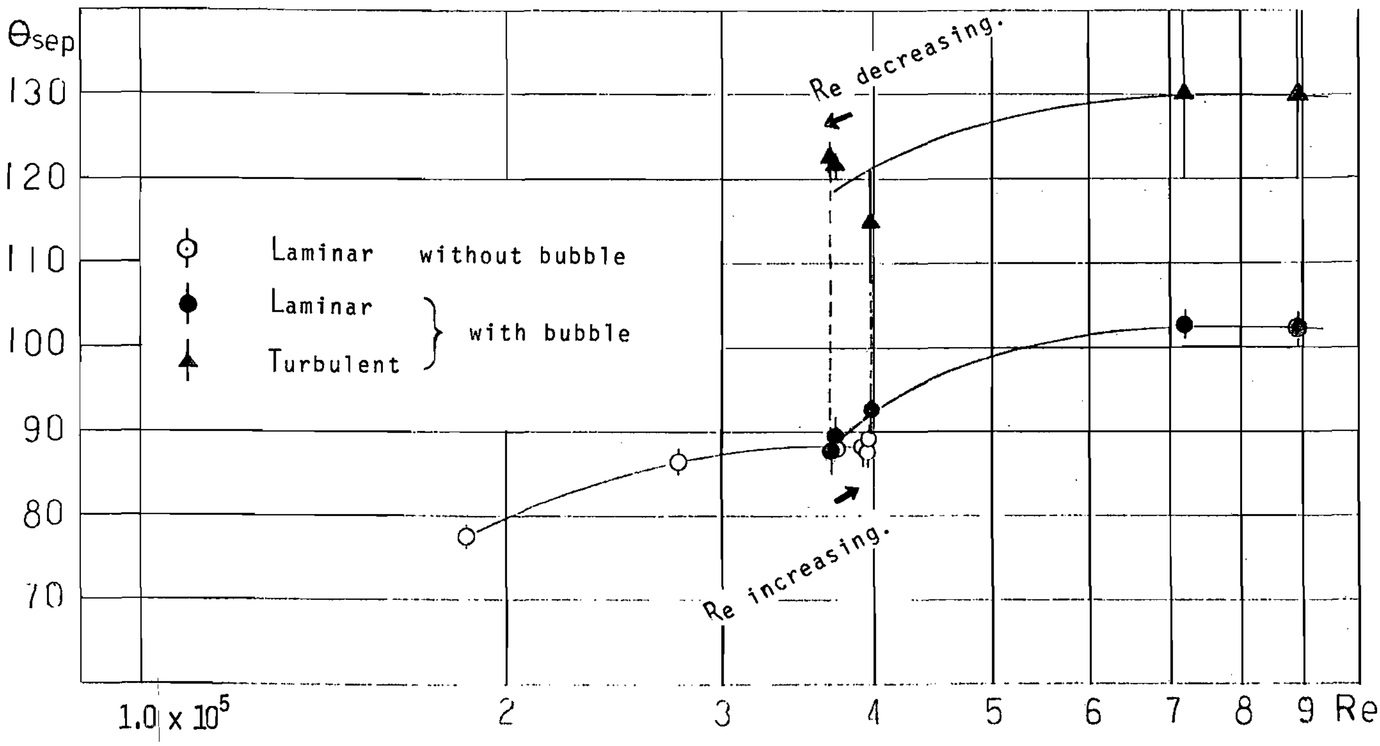

Fig. 14 Variation of the location of separation point of a circular cylinder with the Reynolds number

In the critical range of the Reynolds number, the experiment has been carried out carefully varying wind velocity at intervals of 0.2 - 0.3 m/s monitoring the pressure distribution using multi-tube alcohol manometer in order to catch the Reynolds number where the drag coefficient, C_D, varies discontinuously.

2. Results and discussion

Fig. 11 shows C_D - Re characteristics. C_D varies along the curve A C C' E E' F as the Reynolds number increases and varies along the curve F D' D B B' A as the Reynolds number decreases. C_D varies discontinuously at CC', EE', D'D and B'B and hysteresis phenomenon appears in accordance with the expectation mentioned above.

Fig. 12 shows the variation of the lift coefficient C_L with the Reynolds number. C_L is nearly zero except in the region C'E andB'D, in which the value of C_L is of the order of 1. In Fig. 13 the location of the stagnation point is plotted against the Reynolds number, where θ_{st} is the angular distance of the stagnation point from the leading edge. Fig. 14 shows the variation of the angular distance, θ_{sep}, of the separation point on the upper surface from the leading edge, where θ_{sep} is determined from oil flow visualization. θ_{sep} varies along the axis of the cylinder. The vertical lines show the range of variation. Since pressure measurement has not been made in the case of oil flow visualization, the symbols in this figure do not correspond one to one with the symbols in Figs. 11-13. However the Reynolds number at which discontinuous variation occurs as shown by B'B and EE' in Figs. 11-13 is essentially the same as the Reynolds number at which the jump of the separation point occurs in Fig. 14.

Fig. 15(a), (b), (c), (d), (e), (f) and (g) show pressure distributions along a stream direction corresponding to the points A, B, B', D, D', F and E in Fig. 11 respectively. It is clear from the discussions of Refs. 5 and 11 that (a) and (b) in this figure show the non-existence of a bubble on both surfaces at points A and B (no bubble flow). In this case the value of C_D is about 1 and the value of C_L is essentially zero. (c), (d) and (g) show that a bubble exists only on one surface, and on the other surface the laminar boundary layer separates without attaching again (one bubble flow).

Fig. 13 shows that in this case the stagnation point moves to the surface where bubbles do not exist, resulting in the generation of a lift coefficient of the order of one. The flow is stable and the value of C_D is about 0.4. (e) and (f) show the existence of bubbles on both surfaces at points D' and F (two bubbles flow). In this case the value of C_D is about 0.2 and the value of C_L is essentially zero.

The flow around a circular cylinder in the critical range of the Reynolds number may, therefore, be calssified into three types; no bubble flow, one bubble flow and two bubbles flow in accordance with the result obtained by Bearman(8).

There exist, therefore, four critical values of the Reynolds number corresponding to the boundary of the types of low, they are, $R_{CC'}$ and R_{EE} for increasing Reynolds number and $R_{D'D}$ and $R_{B'B}$ for decreasing Reynolds number, where $R_{CC'}$, for example, is the Reynolds number corresponds to the vertical line CC' in Fig. 11. The type of flow is "no bubble flow" if the Reynolds number is lower than $R_{B'B}$. As Reynolds number increases a bubble forms on one surface at the value of the Reynolds number of $R_{CC'}$ so that the type of flow changes discontinuously to "one bubble flow". The surface, where the bubble forms, changes from a run of the wind tunnel to another run. However once the bubble forms on a surface, the flow becomes stable so that the bubble continues to remain on the surface during the run. The reason for the stabilization of flow is as follows. If a bubble forms on a surface for some reason the stagnation point moves to the side where a bubble does not exist as shown in Fig. 13. The separation point of the laminar boundary layer on the surface without a bubble, however, does not move so much as shown in Fig. 14, resulting in the decrease of the Reynolds number $R_{\delta*}$ based on the displacement thickness of the boundary layer at this point. Then the formation of a bubble on this surface becomes difficult, because the $R_{\delta*}$ is now lower than the critical value of Tani, Owen and Klamfer mentioned in Chapter II, resulting in the stable flow. The formation of bubbles, therefore, does not occur on both surface simultaneously, but occurs only on one surface at first. In Bearman's experiment the bubble formed consistently on the same surface, whereas the surface, where the bubble forms, sometimes changes from a run to another in this experiment. This fact means that the generation of lift is not due to the asymmetry of the geometry of the model or the flow in the wind tunnel. As the Reynolds number increases a bubble forms also on the other surface at the value of the Reynolds number of $R_{EE'}$ so that the type of flow changes discontinuously to "two bubble flow".

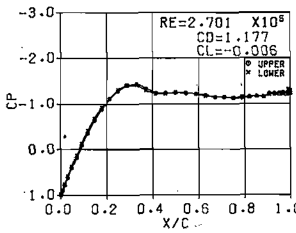

(a) At point A in Fig. 11

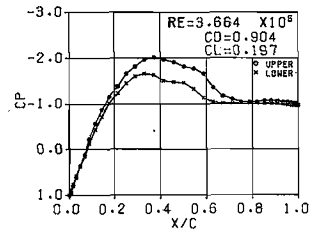

(b) At point B in Fig. 11

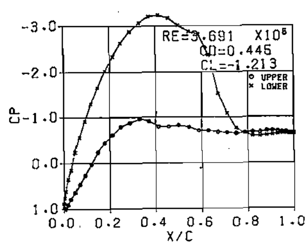

(c) At point B' in Fig. 11

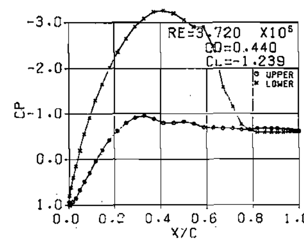

(d) At point D in Fig. 11

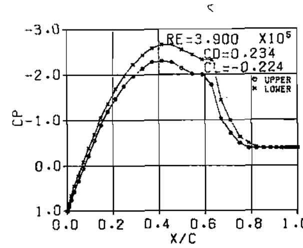

(e) At point D' in Fig. 11

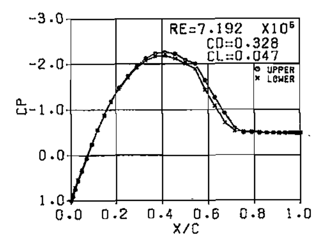

(f) At point F in Fig. 11

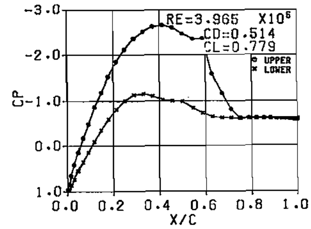

(g) At point E in Fig. 11

Fig. 15 Pressure distribution on a circular cylinder

As the Reynolds number decreases the type of flow changes as "two bubbles flow" → "one bubble flow" → "no bubble flow" discontinuously. The critical Reynolds numbers, at which the type of flow changes, in the case of decreasing Reynolds number is different from those of increasing Reynolds number, resulting in the hysteresis phenomenon.

It is remarkable that in the range of the Reynolds number between $R_{B'B}$ and $R_{EE'}$ two types of flow correspond to one Reynolds number. The type of flow that is realized depends on the history of the flow. The discontinuous variations of C_D and C_L can be considered as those accompanying the jump from one to the other of the two types which correspond to a Reynolds number.

The reason for the continuous variation of C_D of a circular cylinder in the critical range of the Reynolds number as described in text books, would be as follows. In wind tunnels the flow around a circular cylinder is not exactly two-dimensional so that the section drag acting on a section varies along the axis. In the experiments (2)(3)(4) described in textbooks the drag force acting on a cylinder was measured directly by use of a balance so that the section drag force acting on a section was integrated to give continuous variation, although section drag force itself varied discontinuously with Reynolds number as discussed above.

The discussions described so far about the measurement of the aerodynamic force acting on a circular cylinder in the critical range of the Reynolds number are summarized as follows.

1. The C_D - Re and C_L - Re characteristics has been obtained more in detail than those obtained so far.
2. It has been confirmed that C_D and C_L varies discontinuously as the Reynolds number varies.
3. The variations of C_D and C_L in the case of increasing Reynolds number are different from those of decreasing Reynolds number resulting in hysteresis phenomenon.
4. Two types of flow correspond to a Reynolds number. The type which is realized depends on the history of the flow. The discontinuity in the variation of C_D and C_L is considered to be the phenomenon accompanying the jump from one to the other of the two types of the flow.

IV. Aerodynamic Force Acting on a Cone Cylinder

1. Wind tunnel, model, and test conditions

The wind tunnel is the NAL large low speed wind tunnel(10). The height and width of the test section are 6.5M and 5.5M respectively.

Fig. 16 shows a schematic diagram of the model. The model consists of a circular cylinder, the diameter of which is 260mm, and a circular cone having the length to diameter ratio of 5 to 1. Static pressure orifices are installed at five sections, S_1 - S_5 as shown in this figure. In order to measure lift distributions along the axis of the cone, static pressure orifices are installed along two general lines, the angular distance from the leading edge being 80° as shown in Fig. 16(b). Each orifice is referred to as left or right as shown in the same figure.

The model is mounted vertically on the floor. The angle of attack can be varied by a hinge installed at the lower section of the model. Measurements have been made for angles of attack of 90°, 60° and 30°. However only the results for 90° are discussed in this paper. The Reynolds number based on the diameter of the cylinder is increased from 1×10^5 to 1×10^6. There is no experiment with a decreasing Reynolds number.

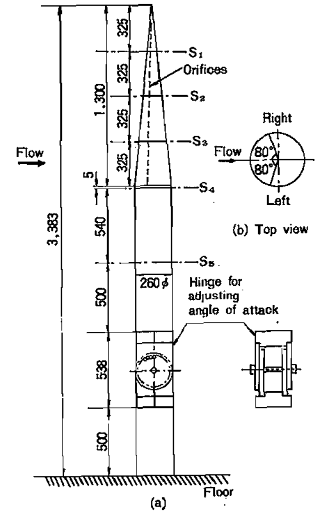

Fig. 16 Schematic diagram of a cone cylinder model

2. Results and Discussion

Fig. 17 shows the variations of the side force coefficient, C_Y, at each section with the Reynolds number, R_D, based on the diameter of each section. At all sections except S_4 the side force coefficient is essentially zero except in a small region of the Reynolds number. At sections S_3 and S_5 the side force appears at small ranges of Reynolds numbers of about 4×10^5 which is close to the critical value of the circular cylinder mentioned in Chapter III (see Fig. 11)

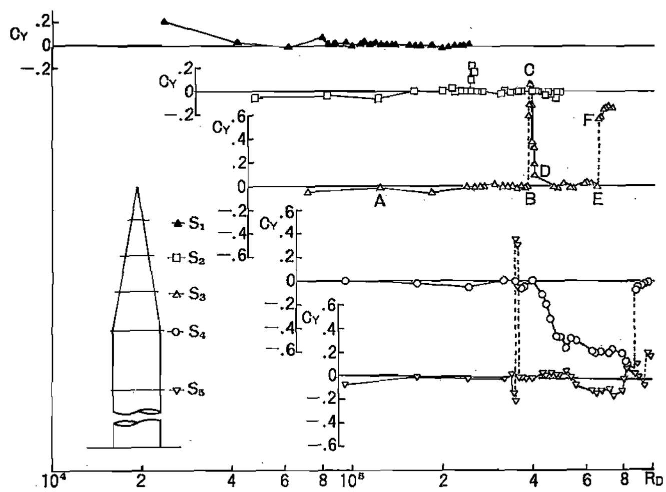

Fig. 17 Variation of section lift coefficient with the Reynolds number, R_D, based on the local diameter of a cone

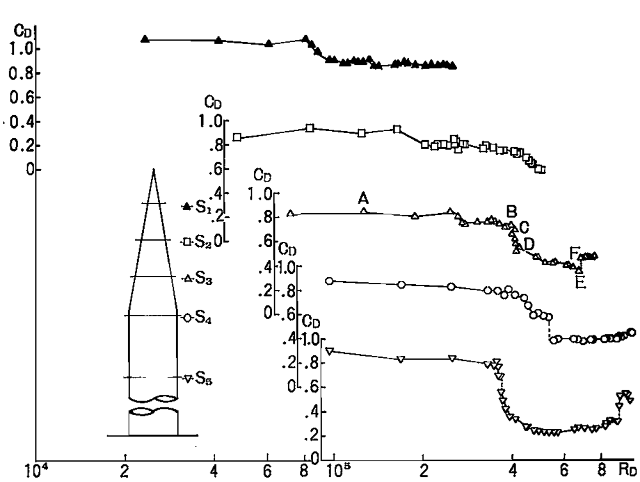

Fig. 18 Variation of section drag coefficient with the Reynolds number, R_D, based on the local diameter of a cone

The variations of the drag coefficient, C_D, are plotted in Fig. 18 an abrupt decrease of C_D appears at the same renges of Reynolds numbers, which suggest that the formation of the bubbles on the right and the left surfaces occurs successively at small intervals of the Reynolds number in this range of Reynolds number.

Pressure distributions of section S_3, at the Reynolds numbers corresponding to points A, B, C, D, E and F, are shown in Figs. 19(a), (b), (c), (d), (e) and (f) respectively. It is clear from the pressure distributions that there is no bubble on the surface at points A and B. At point C a bubble forms on the right surface while the left surface remains without a bubble resulting in a large side force coefficient of 0.860 as shown in Fig. 19(c). At point D the formation of a bubble on the left surface also occurs resulting in the vanishment of the side force as shown in Fig. 19(d). At point E there are bubbles still on both surfaces so that the side force coefficient is nearly zero as shown in Fig. 19(e). The variation of C_Y of this section is so far very similar to that of C_L on the circular cylinder mentioned in Chapter III. At point F, however, a fairly large C_Y appears although bubbles exist on both surfaces as shown in Fig. 19(f).

In Fig. 19 the symbols representing the pressure on the two general lines are located at $x/D = 0.41$. The pressure coefficient on these lines is hereby referred to as Cp_{80}. Fig. 19 shows that Cp_{80} represents approximately the minimum pressure coefficient on the surface. From the value of Cp_{80}, therefore, one knows whether a bubble exists or not on the surface, since the minimum value of C_p on the surface having a bubble is much higher than that without a bubble. Fig. 20 shows the variation of Cp_{80} with the Reynolds number, R_D, based on the local diameter. It is clear that the formation of bubble occurs in the range of R_D around 4×10^5 in accordance with the case of a circular cylinder mentioned in Chapter III.

At a Reynolds number above 4×10^5, based on the diameter of the cylindrical part, there are bubbles on the surfaces of the cone near the corner. Close to the apex, however, there is no

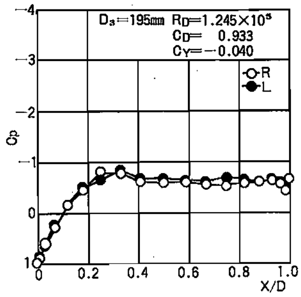

(a) At point A in Fig. 17

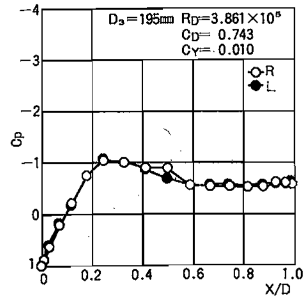

(b) At point B in Fig. 17

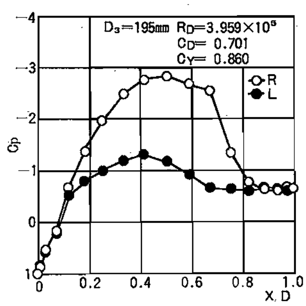

(c) At point C in Fig. 17

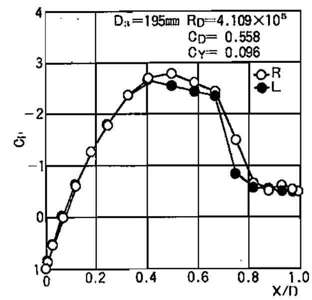

(d) At point D in Fig. 17

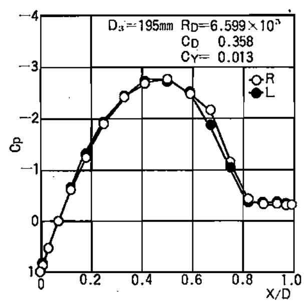

(e) At point E in Fig. 17

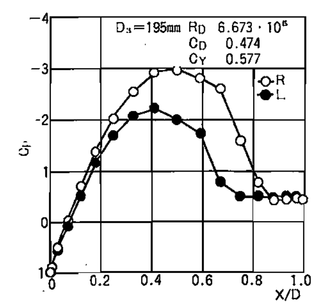

(f) At point F in Fig. 17

Fig. 19 Pressure distributions on the S_3 section

bubble due to a small local Reynolds number, R_D, based on a local diameter. Therefore there exist boundaries between the regions with a bubble and those without. We assume that these boundaries are defined as the location, y_B/L, where $Cp_{80} = -1.6$ holds, where y_B is an axial distance from the apex to the boundary and L is the length of the cone.

In Fig. 21 the location, y_B/L, of the boundaries on the right and left surfaces are plotted against the Reynolds number, Re, based on the diameter of the cylindrical part. The curves representing the relationship between Re and y_B/L for the right and left surfaces are hereby referred to as y_B loci. The locus of the point where $R_D = 4 \times 10^5$ holds is also shown by a solid curve in this figure, where R_D is the local Reynolds number based on the local diameter.

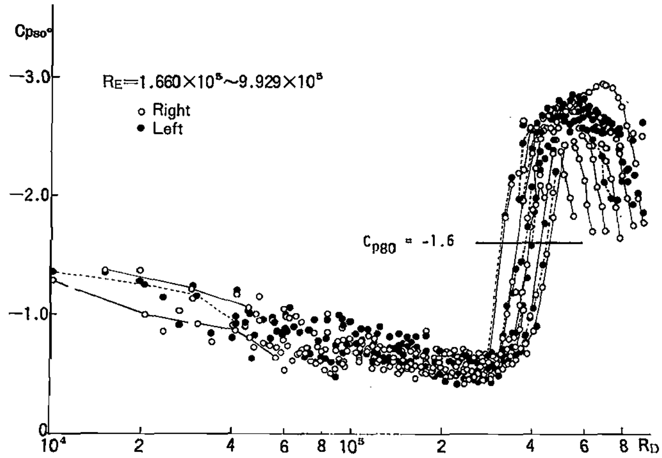

Fig. 20 Variation of C_{p80} with the Reynolds number, R_D, based on the local diameter

If the flow around a section of the cone behaves like a flow around a circular cylinder of the same diameter, the points which represent y_B/L should move approximately along the curve $R_D = 4 \times 10^5$ as Re increases. The points obtained by experiment, however, move slower except for a small region of R_D of about 5.3×10^5 where the movement is abrupt and large.

At the Reynolds number represented by vertical line b in Fig. 21 the boundary on the right surface locates at the apex side of section S_3 while the boundary on the left surface locates at the opposite side. This fact means that at section S_3 a bubble exists on the right surface whereas a bubble does not exist on the left surface. Fig. 22(b) shows the distributions of C_{p80} along the axial distance y/L at this Reynolds number. The figure confirms the above description concerning the existence of a bubble at section S_3.

The side force coefficient C_Y of sections from S_2 to S_5 is plotted against the difference, ΔC_{p80}, between C_{p80} on the right and on the left general lines in Fig. 23. There is approximately a 1 to 1 correspondence between C_Y and ΔC_{p80} so that C_Y can be approximately evaluated from ΔC_{p80}.

Fig. 22(b) shows that a side force acts to the right in the region of the cone between y/L = 0.5 and y/L = 0.85 and it acts to the left in the region where y/L is greater than 0.9, where y is the axial distance from the apex and L is the length of the cone.

Figs. 22(a) and (c) show the C_{p80} distributions at Reynolds numbers represented by vertical lines a and c in Fig. 21 respectively. In both cases the side force does not act except for the region where y/L is greater than 0.9.

In Fig. 21 the regions of the cone where $|C_{p80}| \geq 0.2$, i.e. the side force is appreciable (say, $|C_Y| \geq 0.2$), are shown. In the areas simply surrounded by closed curves without shade, the side force acts to the right and in the shaded arear, vice versa. The side force appears in the sections close to the shoulder of the cone cylinder (y/L = 1) and the sections close to the y_B locus shown in Fig. 21.

At $y = y_B$, namely at $C_{p80} = -1.6$, $dC_{p80}/d(y/L)$ is very large as shown in Fig. 20, so that small

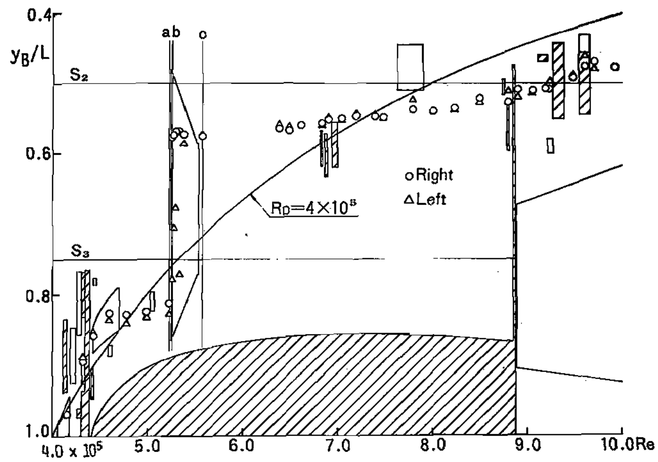

Fig. 21 Variation of the axial location of the bodundary of the region, where bubble exist, with the Reynolds number, Re, based on the diameter of the cylinder. And the region where appreciable section side force coefficient ($|\Delta C_{p80}| \geq 0.2$) exists

Shaded region; side force acts to right
Region simply surrounded by a closed curve; side force acts to left

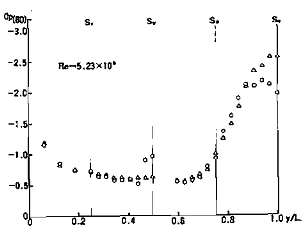

(a) At line "a" in Fig. 21

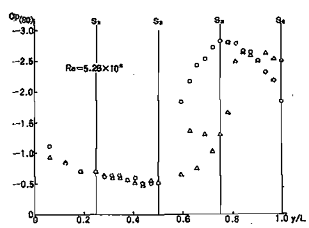

(b) At line "b" in Fig. 21

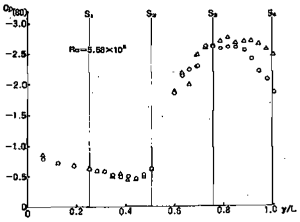

(c) At line "c" in Fig. 21

Fig. 22 Variation of C_{p80} with axial location

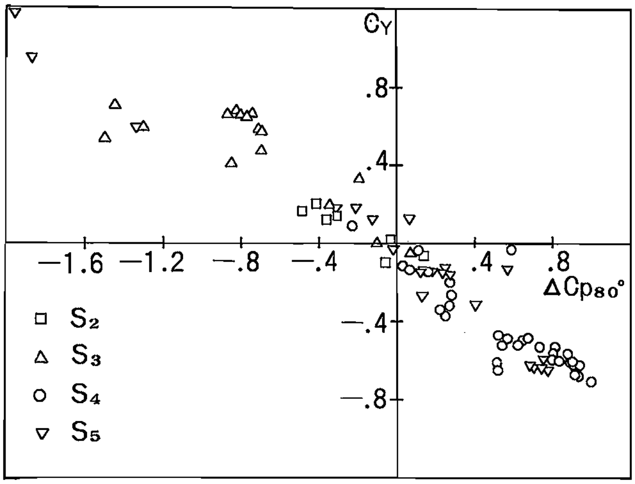

Fig. 23 Relationship between section lift coefficient and ΔC_{p80}

difference between the value of y_B on the right surface and that on the left surface yields appreciable value of ΔC_{p80} or side force coefficient C_Y. This fact is the reason for the existence of the regions of appreciable side force close to the y_B locus. The side force acting on the sections in this region is, therefore, due to the asymmetry of the formation of bubbles, which the authors expected to be the origion of the flat spin experienced at the air drop test of a sounding rocket payload models. Whereas the side force acting on the sections close to the shoulder is probably due to the asymmetry of the behavior of turbulent boundary layers. The former side force appears intermittently in contrast to the consistent appearance of the latter as shown in Fig. 21. Therefore the side force due to the asymmetry of the bubble formation could partly be the origin of the flat spin at some Reynolds number, although the main origion would be the side force acting on the sections close to the shoulder.

V. Concluding Remarks

Several results have been described of experiments on the phenomena including the burst and the formation of laminar separation bubbles. These phenomena are characterized by discontinuity, hysteresis and asymmetry, they are:

1. The type of flow changes discontinuously as the Reynolds number varies.
2. The Reynolds number at which the above discontinuous change occurs is different depending on whether the Reynolds number is increasing or decreasing, resulting in hysteresis phenomena.
3. The flow sometimes becomes asymmetric even if the geometry of the body is symmetric.

Acknowledgement

The authors would like to express their appreciation to Professor I. Tani for his valuable advice.

References

1. Gault, D.E., "A correlation of low-speed, airfoil-section stalling characteristics with Reynolds number and airfoil geometry", NACA TN-3963, (1957).

2. Relf, E.F., "Discussion of the results of measurements of the resistance of wires, with some additional tests on the resistance of wires of small diameter", ARC R&M 102, (1914).

3. Wieselsberger, C. et al., "Ergebnisse der aerodynamischen Versuchsanstalt zu Göttingen", II Lieferung, pp.23-28, (1923).

4. Fage, A. and Warsap, J.H. "The effects of turbulence and surface roughness on the drag of a circular cylinder", ARC R&M 1283, (1930).

5. Roshko, A., "Experiments of the flow past a circular cylinder at very high Reynolds number," J. Fluid Mech. Vo. 10, pp.345-356, (1961).

6. Achenbach, E., "Distribution of local pressure and skin friction around a circular cylinder in cross flow up to Re = 5 x 10^6", J. Fluid Mech. Vol. 34, pp.625-639, (1968).

7. I. Tani, "On the periodic shedding of vortices from a circular cylinder at high Reynolds numbers", Paper presented at the IUTAM Symposium on Concentrated Vortes Motions in Fluids, (1964).

8. Bearman P.W., "On the vortex shedding from a circular cylinder in the critical Reynolds number régime", J. Fluid Mech., Vol. 37, pp.577-585, (1969).

9. Shirouzu, M., Kubota, H. and Shibato, Y., "Aerodymanic aspects on recovery of sounding rocket payload", Preprint for XXXI IAF Congress, Pergamon Press. (1980).

10. Sigemi, T. and Hirooka, K., "6m Low-speed Wind Tunnel at the National Aerospace Laboratory (in Japanese)", J. Japan Soc. Aero. Space Sci., Vol. 15, No. 167, pp.408-417, (1967).

11. Tani, I., "Low speed flows involving bubble separations", Progress in Aeronautical Sciences, Vol. 5, pp.70-103, Pergamon Press, (1964).

12. Thwaites, B., "Approximate calculation of the laminar boundary layer", Aero. Quart. Vol. 1, pp.245-280, (1949).

13. Tani, I., "Note on the interplay between the laminar separation and the transition from laminar to turbulent of the boundary layer (in Japanese)", J. Soc. Aero. Sci. Japan Vol. 6, pp.122-134, (1939).

14. Owen, P. R. and Klanfer, L., "On the laminar boundary layer separation from the leading edge of a thin aerofoil", ARC CP220 (1955).

15. Hirosue, K., Kitamura, K., Murakami, Y. and Shindo, S., "Design and development of the gust wind tunnel at the National Aerospace Laboratory (in Japanese)", NAL TR-335, (1973).